UNIVERSITY OF CALIFORNIA SAN DIEGO

Design of Electronics for Wearable Electrochemical Sensors

A Thesis submitted in partial satisfaction of the requirements
for the degree Master of Science

in

Electrical Engineering (Medical Devices and Systems)

by

Christopher Brown

Committee in charge:

Professor Joseph Wang, Chair
Professor Shadi Dayeh, Co-chair
Professor Tina Tse Nga Ng

2019

The Thesis of Christopher Brown is approved, and it is acceptable in quality and form for publication on microfilm and electronically:

_____

_____

Co-chair

_____

Chair

University of California San Diego

2019

TABLE OF CONTENTS

LIST OF ABBREVIATIONS

Microcontroller ..... MCU
Digital to Analog Converter..... DAC
Analog to Digital Converter..... ADC
Transimpedance Amplifier ..... TIA
Counter Electrode ..... CE
Reference Electrode ..... RE
Working Electrode ..... WE
Cyclic Voltammetry CV
Square Wave Voltammetry ..... SWV
Electrical Impedance Spectroscopy ..... EIS
Printed Circuit Board ..... PCB
Inter-Integrated Circuit I2C
Bluetooth Low Energy ..... BLE
Linear Dropout Regulator ..... LDO
Prussian Blue ..... PB
Interstitial Fluid..... ISF

LIST OF FIGURES AND TABLES

ABSTRACT OF THE THESIS

Design of Electronics for Wearable Electrochemical Sensors

by

Christopher Brown

Master of Science in Electrical Engineering (Medical Devices and Systems)

University of California San Diego, 2019

Professor Joseph Wang, Chair
Professor Shadi Dayeh, Co-chair

There is a growing need for accurate, wearable electrochemical sensors for use in a large range of industries including medical, fitness, military, environmental and food. The wearable medical device market has traditionally been dominated by activity trackers [1]; however, the conclusion of the Apple Heart Study and subsequent FDA approval of a watch based electrocardiogram shows the expansion of the wearable medical device market [2]. This work presents a generalized set of guidelines that can be followed to design wearable electrochemical sensing systems at a high technology readiness level. Specific emphasis is placed on the engineering tradeoffs involved in the design of the electronics and the sensing of biomedically

important analytes. These guidelines are used as a blueprint in the development of a minimally invasive continuous glucose monitor. This system is tested and analyzed to confirm that it is operating as intended. The continued development and widespread adoption of wearable electrochemical sensors has the potential to provide a wealth of bioanalytical information which could have a tremendous impact on healthcare systems.

Introduction

Wearable electrochemical sensors provide a cost effective method for detecting a wide variety of personal and environmental analytes ranging from glucose to airborne nerve agents [3, 4]. Electrochemical sensors exhibit excellent selectivity from a wide variety of selective coatings that can be applied to the surface of their electrodes [5]. Sensors can be built atop a range of substrates with shapes and sizes tuned by application. The flexibility offered by electrochemical sensors makes them an ideal candidate for sensing biomedical analytes in wearable devices.

As the design and development of new wearable sensors continues, the associated measurement and control system must continue to adapt to the changing requirements of sensors and new applications. In analytical electrochemistry the system of choice is the potentiostat. A potentiostat is used to control the potential between a pair of electrodes in an electrochemical cell. A potentiostat maintains control through the injection of current into the cell. In potentiostatic experiments the cell potential is the independent variable and the cell current is the dependent variable.

Generally, a wearable potentiostat will have the following subsystems: a disposable sensor, a quick-connect sensor interface, a potentiostatic control circuit, a digital to analog converter to produce the control signal, a current to voltage converter to transform the electrochemical current into a measurable voltage, an analog to digital converter to digitize this voltage, a microcontroller (MCU) orchestrating the measurements and analyzing the data, a communication interface to relay the data to users, and a battery and regulator to provide power to all systems. These subsystems are their connections are shown in Figure 1.

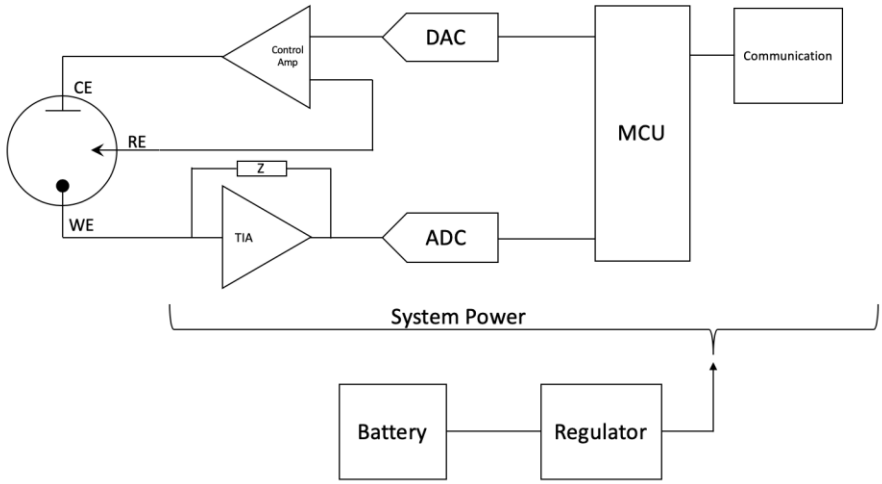

Figure 1: Electrochemical Sensing System. System components include the counter electrode, reference, electrode working electrode, control amplifier, transimpedance amplifier, digital to analog converter, analog to digital converter, battery, voltage regulator, microcontroller, and communications.

Electrode Design

Electrodes provide the electrical interface needed to analyze chemical changes and to monitor the production of electrical energy in chemical reactions. A single electrode is of little use in the study of analytes as there is not a completed path for electrons to flow. These electrons flow to balance the movement of charge that occurs in a reaction. To create this conductive pathway, electrodes must be combined to form electrochemical cells consisting of an anodic electrode, cathodic electrode, and an electrolyte [6]. Electrochemical cells are classified into two groups – electrolytic and galvanic. Galvanic cells undergo spontaneous redox reactions which generate electric energy. Electrolytic cells drive non-spontaneous redox reactions when a potential larger than the open circuit voltage of the cell is applied. Potentiostats rely on electrolytic cells for their analysis of analytes. In electrolytic cells, the anodic electrode is where the oxidation reaction occurs at the interface between the electrode and electrolyte. The cathodic electrode is defined as the electrode which undergoes reduction. When the anode and cathode are combined the cell forms a complete redox process.

In a sensing system, the redox process should be designed so that the analyte of interest is the limiting factor in the reaction. This is done by tuning the performance of the electrodes in the cell so that reaction of interest occurs at the working electrode interface. The counter electrode serves to balance the redox process and complete the circuit but should not have a limiting effect on the reaction. Electrode performance is turned primary by three parameters – size, material, and decoration. In order to ensure that the reaction at the working electrode is the limiting factor in the redox process, the counter electrode is often larger than the working electrode. This larger interface supports more charge transfer than the smaller electrode. It is also beneficial to fabricate the counter electrode from an electrochemically inert material like carbon, gold, or platinum. Inert materials have an equal anodic and cathodic current, so no bias is introduced when utilizing both positive and negative stimulation. This charge balancing is desirable as it prevents the buildup of reaction byproducts in the cell. The working electrode material can be chosen to directly react with the analyte of interest, but for most analytes it is simpler to decorate an inert working electrode with an ion or molecule selective coating. These coatings are used to ensure high selectivity of analytes in the redox reaction.

Charge Transfer

Charge can be transferred across an electrode interface by two methods: faradic and non-faradic charge transfer. In a faradic process charge is transferred across a metal-solution interface and oxidation or reduction occurs. In these reactions, the rate of the chemical reaction caused by the flow of current is proportional to the amount of electricity passed [7]. In some cases, charge transfer will not occur because the reaction is unfavorable either thermodynamically or kinetically. However, processes like absorption and desorption can still occur which cause a change to the capacitive double layer at the electrode surface. This changing potential can drive

external currents at the electrode [7]. The best criteria for identifying a faradic process is by evaluating the electrode composition given a constant current supply. If the electrode composition changes then this is a faradic process [8]. In a non-faradic process, there is a storage of charge in the capacitive double layer immediately surrounding electrode. This structure is formed as the potential in the electrode repels the co-ions while attracting the counter ions of the solution. These inner ions are held tightly to the electrode by electrostatic forces and arrange themselves into an aligned array. This layer then attracts another layer of ions. Together these layers form a parallel plate capacitor at the surface of the electrode. While there are benefits in stimulation applications to non-faradaic process, faradaic processes are typically preferred for sensing applications because they relate reaction rates with analyte concentration.

Reaction Rate and Current

A faradaic redox reaction occurring at an electrode is governed by a variety of factors which control the reaction rate and current. The current generated by this reaction is directly proportional to the rate of the chemical reaction occurring at the electrode [7]. This relation is described by Faraday's Law of Electrolysis shown below [9]:

$$m = \frac{QM}{nF}$$

In this equation the variables are defined as follows:

- m – mass of the substance liberated at the electrode (grams)
- Q – total charge carried through the substance (coulombs)
- F – Faraday's Constant (coulombs per mol)
- M – molar mass of the substance (grams per mol)
- n – valence number of ions in the substance

This reaction can be adapted to the form shown below to express the relationship between the reaction rate and the resulting current density. Here t is time, i is current, A is area and j is current density.

$$Rate\left(\frac{mol}{s\ cm^2}\right) = \frac{i}{nFA} = \frac{j}{nF}$$

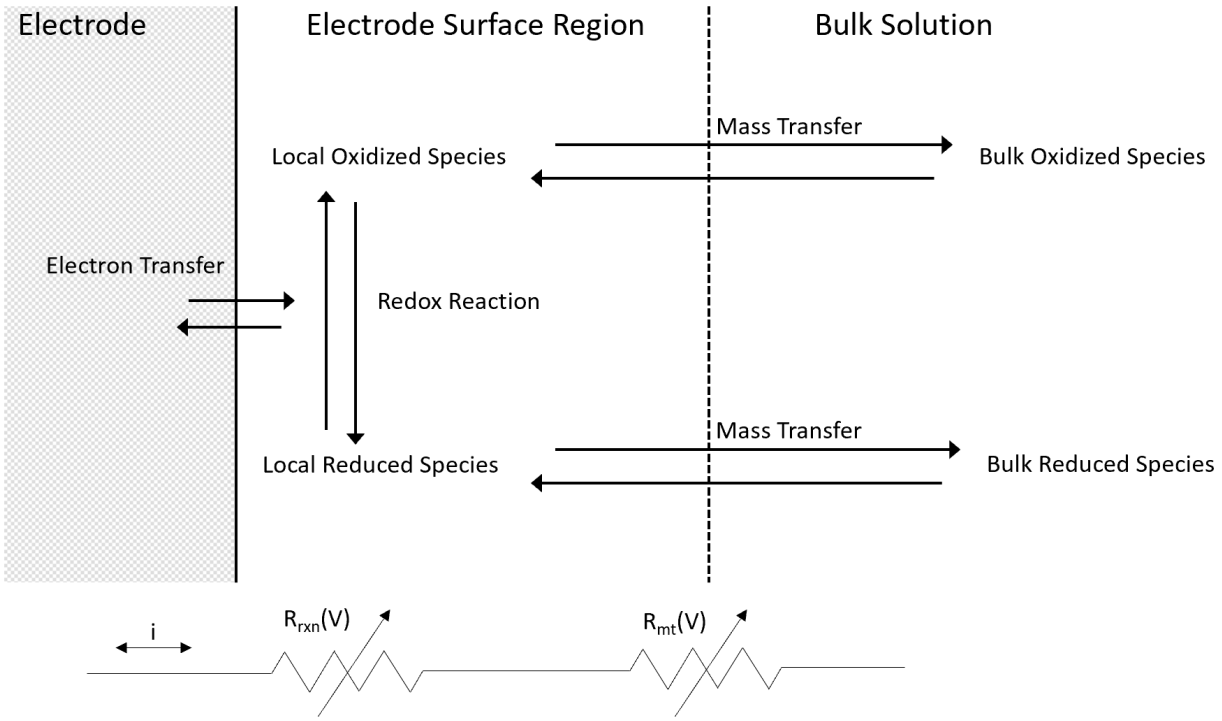

Figure 2: Reaction pathway for simplified electrode reaction. Adapted from [7].

In the simplest redox reaction, there are three potential rate limiting factors. These factors are the mass transfer of the oxidized species, the reaction kinetics of the electron transfer, and the mass transfer reduced species. Each of these processes is voltage dependent and they can be modeled as a series of voltage dependent resistors. The overall reaction rate is the sum of these resistances. A reaction is held back by the limiting element in this series. When this element is the electron transfer, the reaction is considered kinetically limited. A reaction is considered mass transport limited when the electron transfer rate is faster than the mass transport rates: as soon as

new species arrives from the bulk solution; they immediately react transferring electrons with the electrode.

There are three modes of mass transport:

- Diffusion of the analyte between the bulk solution and the electrode interface due to a concentration gradient.
- Convection of the analyte due to mechanical or hydrodynamic means.
- Migration of charged species due to a potential gradient.

Mass transport is modeled by the Nernst – Planck equation. In one dimension the equation is defined as follows [7]:

$$J_i(x) = -D_i \frac{\partial C_i(x)}{\partial x} - \frac{z_i F}{RT} D_i C_i \frac{\partial \phi(x)}{\partial x} + C_i v(x)$$

The three terms on the right-hand side of the equation are the three modes of mass transfer. For more information and a complete derivation see [7]. The diffusion control mode of a mass transport limited reaction is desired in amperometric measurements. This is achieved by eliminating the effects of migration and convection on the reaction. Under these conditions the Nernst – Planck equation reduces to the following form:

$$J_i(x) = -D_i \frac{\partial C_i(x)}{\partial x}$$

This reduced form expresses the flux of species i, $J_i(x)$, as a function of the product of concentration gradient, $\frac{\partial C_i(x)}{\partial x}$, at position x and the diffusion coefficient D_i.

A simple amperometric measurement begins with the application of the redox potential to the electrochemical cell. This potential increases the redox reaction rate (or lowers the resistance

of R_{rxn}, Figure 2) which drives the concentration of the localized species to zero and creates a diffusion limited reaction. The diffusion rate is related to the concentration gradient through the equivalence of the Faraday's Law of Electrolysis and the Nernst – Planck equation. Since the concentration at the electrode interface is essentially zero, the gradient is only dependent on the bulk concentration. As a result, measured current is linearly related to the bulk concentration of the species of interest. This detection pathway is the foundation for many biosensors with analytes including glucose, lactate and biomarkers indicative of cancer and sepsis [10-13].

Two Electrode System

The two-electrode system is the simplest experimental setup that is capable of preforming electrochemical experiments. When studying an analyte there are two primary parameters of interest – cell potential and current. Experiments are generally conducted by using change in potential to disrupt the equilibrium of the system. The electrochemical cell's current flows between the working and counter electrodes. The chemical reaction of interest occurs on the interface of the working electrode and the resulting current can be measured at either the working or counter inputs. Since only two electrodes are available, the counter electrode performs two functions – it provides a path for current to flow and maintains the cell's potential independently of the current. Unfortunately, the currents flowing at the counter electrode cause the potential to change making it difficult to maintain a stable potential. Solution resistance can also cause unintended changes to the cell potential. If the cell in Figure 2, was used in a two-electrode configuration the potential between the counter electrode (CE) and working electrode (WE) would be measured. The potential profile shows that the measurement will contain artifacts from the solution resistance and CE double layer, in addition to the drop that occurs over the region of interest near the working electrode.

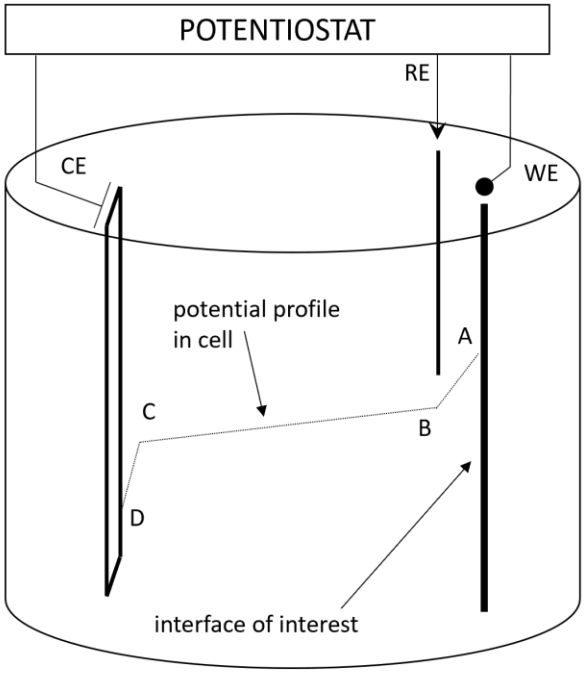

Figure 3: Potential profile in electrochemical cell

Three Electrode System

The issues with the two-electrode system are resolved by adding an additional reference electrode [14]. This electrode provides an isolated and stable reference which is used while measuring the potential. The reference electrode is designed to act as only a potential reference and does not carry any significant current. In order to minimize the voltage difference at the surface of the reference electrode a low impedance electrode is desired. The three-electrode system provides two main advantages over the two electrode system – the reference electrode is not effected by current that flows in results to a change in potential and it can be small, since it doesn't need to carry current, which allows it to be placed very close the working electrode. This minimizes the drop in potential caused by solution resistance. The potential drop caused by solution resistance causes a problem in in two electrode systems since the potential must be measured between the counter and working electrodes. The applied potential provides

critical information for analysis. The solution resistance and the resulting potential drop are a source of error in measurements and should be compensated for when possible.

Measurements Techniques

There are a wide variety of electrochemical measurement techniques that can be performed with commercial potentiostats. While measurement flexibility is a desirable characteristic for commercial potentiostats, it is often cast aside to make systems smaller and cheaper. System size is critically important in wearable sensing systems since a major design goal is to make the system minimally intrusive. As a result of this tradeoff wearable systems often support only a single measurement technique. This is an acceptable reduction in functionality since preliminary experiments are used to identify the best measurement technique for sensing a particular analyte prior to the design of the wearable potentiostat.

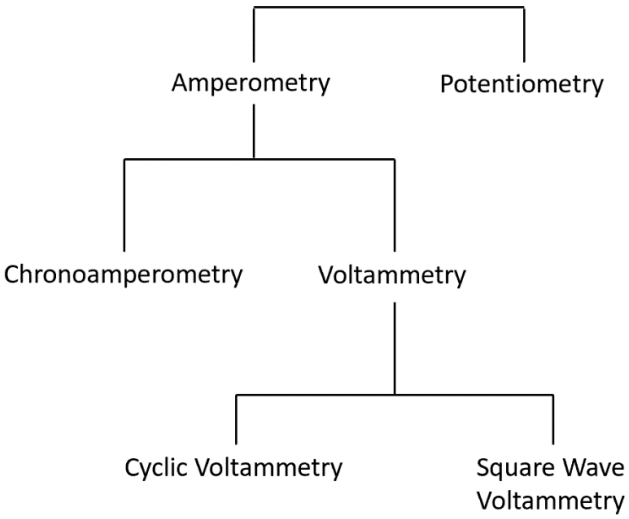

Figure 4: Tree of electrochemical measurement techniques

Figure 4 is a tree showing the relationship between four common measurement techniques – potentiometry, cyclic voltammetry (CV), square wave voltammetry (SWV), and chronoamperometry. A potentiometric measurement technique is one where the potential of the electrochemical cell is directly measured. This potential is measured between the reference electrode and the working electrode. This is contrasted with the amperometric family of measurements that measure current while controlling the cell potential.

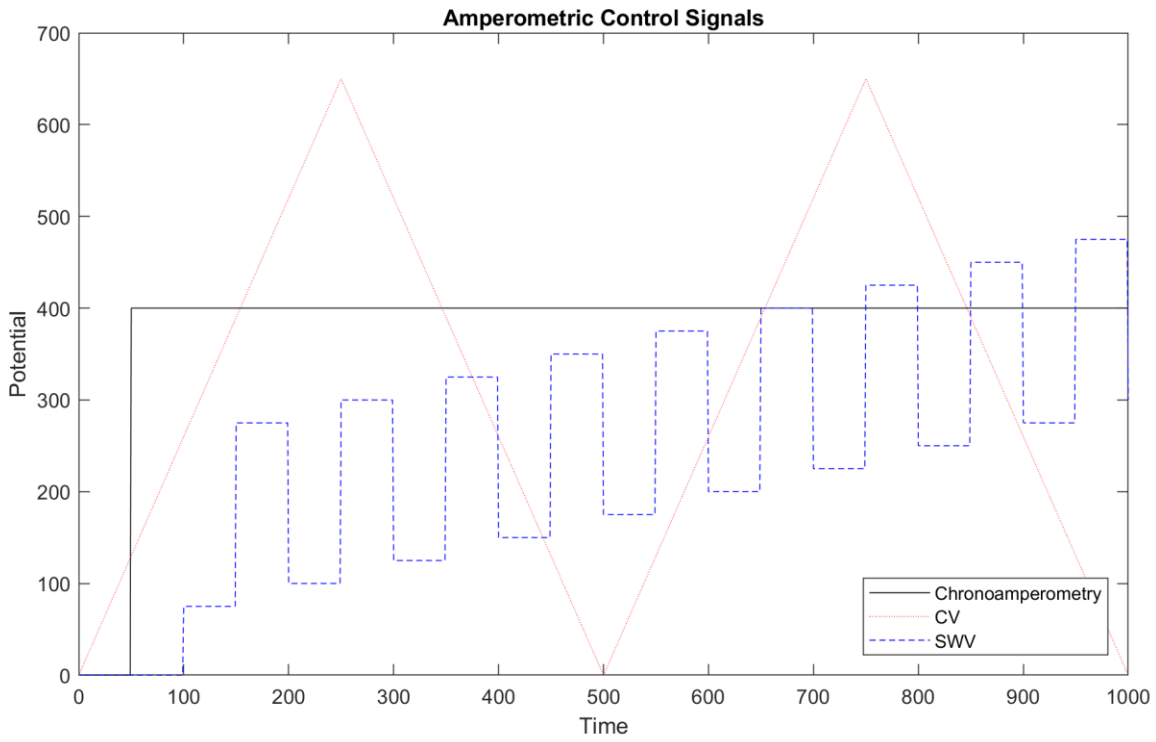

Figure 5: Control Signals for amperometric measurement techniques

Chronoamperometry is a powerful tool for measuring diffusion-controlled reactions. In chronoamperometry the potential is stepped at the beginning of the experiment and then remains constant throughout the duration of the measurement. The current that results from this stimulus is plotted as a function of time. Voltammetry techniques vary the potential as a function of time. The resulting current is plotted as a function of potential. CV sweeps the potential of the cell

linearly across a voltage range. This sweep is performed in both the positive and negative direction and is often conducted more than once. Adjusting the sweep rate between measurements allows the reversibility of the redox couple to be analyzed. Peaks in the CV curve are indicative of redox processes and peak amplitude is used to determine concentration. If a redox couple is present in the sweep window both an anodic and cathodic peak will be observed. If the two peaks are similar in size and shape this indicates that the redox reaction is reversable or, to put it differently, that the reduced analyte is being re-oxidized. SWV uses a square wave superimposed over a staircase function to provide a sweeping measurement that provides two sampling instances per potential. As a result of this sampling technique, the contribution to the total current that results from the non-faradic current is minimized. Like CV, the current is plotted as a function of potential.

General Methods

Introduction

Modern potentiostats are by nature, mixed signal systems. Most wearable potentiostats systems will share the following subsystems – potentiostat, potential control/control signal generation, transimpedance amplifier, and measurement/digitization. The implementation of each of these subsystems will determine the performance of the sensing system. These subsystems should be realized on a printed circuit board (PCB) which is housed inside of a user-friendly enclosure. This section outlines a system architecture and component selection processes that can be used to create sensing platforms that are capable of performance like commercial bench top systems.

Potentiostat Circuit

The potentiostat circuit is the namesake element of the potentiostat and is used to control the potential in an electrolytic cell by adjusting the current flowing through the counter electrode. In a typical three electrode configuration, the potential is controlled between the reference electrode and the working electrode while the current is monitored at the counter electrode. A simple potentiostat circuit shown in Figure 1. The control amplifier uses a single op-amp with the reference electrode in the negative feedback loop. This allows the op-amp to drive the current required to compensate for the potential lost due to solution resistance between the counter and reference electrodes. This is shown graphically in Figure 3. Here the potentiostat is compensating for the drop-in potential from point B to point D.

The choice of op-amps in the potentiostat circuit play a critical role in defining the system limitations. The op-amps (Figure 6: U1- U2) were selected to minimize potential control inaccuracies, and to have a wide enough bandwidth to support required measurement techniques. The input bias current of the buffer (Figure 6: U2) at the reference electrode should be minimized in order to maintain a stable reference. In general, the current flowing into the reference electrode must be minimized. This is done electrochemically though the selection of the electrode, but care must also be used to keep the input bias current small, which is summed with the reference electrode current at the input of the op-amp, to maintain a minimized reference current.

The potential control accuracy of potentiostat circuit is also affected by the voltage noise density of the op-amps. As you may expect, it is desirable to minimize the noise over the frequencies of interest. Although the resulting current from the electrochemical cell will be a low frequency signal, the frequency of the control signal can vary widely depending on the

measurement technique chosen. For example, chronoamperometry requires a DC control signal which holds the cell at a fixed potential while electrochemical impedance spectroscopy (EIS) may require modulation frequencies in the megahertz range. The bandwidth of the control and buffer (Figure 6: U1, U2) op-amps must be wide enough bandwidth to support these measurements.

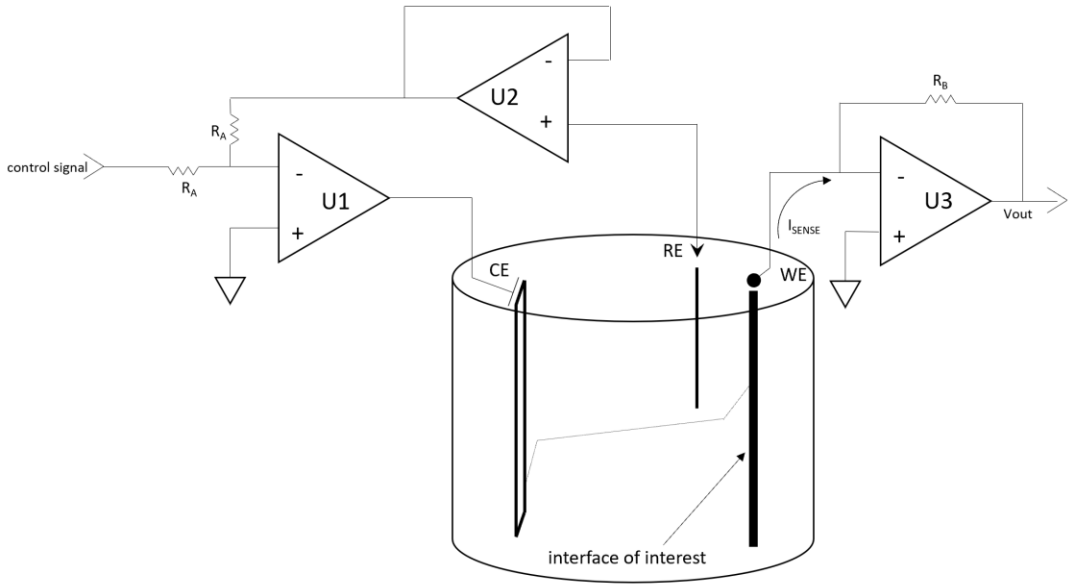

Figure 6: Electrochemical cell with op-amps

Electrochemical measurement techniques require different patterns of potential modulation at the working electrode. Three commonly used modulation schemes are described below:

1. Chronoamperometry – Constant potential is maintained at the working electrode. Current is plotted as a function of time.
2. Cyclic Voltammetry – Potential at the working electrode is swept in a cyclic pattern (Ex. 0 V – 1 V, 1 V – 0 V). Current is plotted as a function of potential.

3. Square Wave Voltammetry – A square wave is superimposed on a linear staircase signal and swept linearly. Current is plotted as a function of potential.

The simplest way to accommodate this wide variety of control modulation is with the use of a digital to analog converter (DAC). The DAC allows a digital microprocessor to generate the needed analog signals for these measurement techniques. The DAC is a discrete time device and generates a staircase signal in response to it digital control signal. The accuracy of this signal is primarily impacted by the resolution of the DAC. It is preferable to use a high-resolution DAC to generate an accurate control signal. This staircase signal is generated at the DACs sample rate and results in the generation of aliases of the signal at frequency multiples of the sampling frequency. For low frequency measurement techniques, these aliased versions of the control signal will not have a large impact since the signal is relatively constant. However, in techniques that employ scanning or high frequency switching (ex. CV, EIS) the aliasing may impact the control signal by adding unwanted high frequency content. To prevent the aliasing from impacting the measurement, an anti-aliasing or reconstruction should be employed. This filter can be implemented using a wide range of architectures so long as it can remove the aliased content while minimizing the impact on the true signal.

Measurement

In addition to controlling the potential of the electrolytic cell the potentiostat must be able to monitor the resulting current. At the core of the measurement system is the analog to digital converter (ADC). The measurement accuracy is directly impacted by the resolution of the ADC due to quantization error. To minimize quantization error an ADC with a high resolution should be selected. Most commercially available, high resolution ADCs cannot directly measure current. To measure the current, it must first be converted to a voltage. Due to the small currents that

need to measured and a need for high accuracy, a transimpedance amplifier (TIA) is used [15, 16]. The output of the transimpedance amplifier is linearly proportional to the input current. In Figure 6, the output voltage of the transimpedance amplifier is related to the input current with the following equation: $V_{out} = I_{SENSE} * R_B$. This simple relationship makes gain adjustments to the sensing system simple. With the change of one resistor the measurement range of the system can be tuned for the desired application. The TIA also presents a high input impedance that prevents loading of the sensor.

Like the control amplifiers used in the potentiostat circuit, the performance of the TIA is also highly dependent on the op-amp chosen. The primary concern for the op-amp used in the TIA (Figure 6: U3) is the input bias current. To minimize input bias error the op-amp selected must have an extremely small input bias current. Typical currents measured by wearable potentiostats for biomedical sensing applications approximately range from nanoamps to tens of microamps. The input bias current is added to the current of interest (resulting from the electrochemical cell) before being amplified and sent to the ADC. If the input bias current is near the measurement current range, it will cause significant error in the measurement and may even saturate the amplifier. To minimize the impact of the input bias current on the measurement, it should be as small as possible. For example, if a TIA has been designed for use in a 3 V system with a maximum expected current of 100 nA. A conservative feedback resistance value in the TIA would be 3 MΩ. In the absence of input bias current, the amplifier will not saturate until the input current is 10X (1 µA) the expected current. However, if the selected op-amp has an input bias current of 45 nA (input bias current of the common LM321 op-amp) the 10X saturation margin will be reduced to 6.8X. In applications with lower electrochemical currents more aggressive amplification is needed and the impact of the input bias current increases.

The capacitive double layer of the electrode can create a significant capacitance at the input of the TIA. The TIA must be designed so that it is stable when this large capacitance is present. Stability is commonly improved with the addition of a feedback capacitor which is in parallel with the feedback resistor. The same capacitance will also appear at the output of the control amplifier. In both cases care must be taken to provide ample phase margin to prevent op-amp instability.

System Control and Communication

The potentiostat and measurement subsystems must be controlled in order to execute the various measurement techniques. In wearable systems, the component of choice for this task is a microcontroller (MCU). MCUs are capable of low power operation and are available with a wide range of feature sets and communication interfaces. To simplify the system, it is desirable to choose an MCU that implements the needed communication interface. The most common choices for measurement systems are Bluetooth Low Energy (BLE) and the Universal Serial Bus (USB). BLE is preferred for wearable devices because of its low power consumption and ample range. Wireless communication leads to a less obtrusive system that is easier to use and allows for integration with advancing healthcare networks. Wireless sensors can be autonomously monitored to provide real time alerts and analyze long-term trends. Wearable, wireless medical devices will enhance the efficiency of our healthcare system. The many benefits of wireless communication require that an MCU with integrated BLE radio be used.

The MCU also provides other options for higher levels of system integration. Many MCUs also have integrated ADCs and DACs. These devices can be used to replace the dedicated DAC and ADC used in the potentiostat and measurement subsystem. However, this change should only be made if the sensing system can tolerate the reduction in accuracy that will likely

result. MCUs are general devices and do not have high resolution ADCs and DACs. If a standalone ADC and DAC are used, the MCU must have the digital communication interfaces needed for communication with these devices. The BLE communication interface and all system behavior is implemented in the firmware which runs on the MCU. This code is written in C and is programmed onto the MCU. In space constrained applications this interface can be implemented on a breakaway portion of the PCB for removal after programming. The MCU selected should also be capable of low power operation to minimize the size of the battery used. Additional features of interest that are offered in some MCUs are over-the-air firmware updates and programmable analog blocks.

Power

The choice of the power supply and regulators in the system determine the system runtime and the measurement range. Lithium ion batteries provide a high specific energy (Wh/kg) and ample specific power (W/kg) for this application [17]. The high specific energy of li-ion batteries helps to reduce system size. Lithium ion batteries are also widely available and cost effective which makes them well suited for most designs. The main limitation of lithium ion batteries is the reduction in capacity due to repeated charge-discharge cycles. Supercapacitors provide a better option for energy storage in devices that require a high frequency charge-discharge cycle. For example, if the system is relying on energy harvesting instead of a battery, the storage element may be cycled often as the electronics consume the entirety of available energy each time it is charged. This scheme is required to run the harvesting system at the maximum measurement rate.

Regardless of the energy storage element, the system must be capable of measuring the required analytes. This requires a constant regulated power supply with minimal noise. Reducing

the noise on the power supply is important to reduce noise in the analog signals and to provide a stable reference for the analog circuitry. Supply noise is minimized with low noise regulators and additional filtering. Most biomedical analytes are measured in aqueous solutions which limits usable potential range of the electrolytic cell to 1.23 V due to the electrolysis of water [18]. Outside of this potential range water is split into hydrogen and oxygen. Electrolysis causes biocompatibility issues due to the release of oxygen and hydrogen gas. By modifying the pH of the aqueous solution, the potential window can be extended to 3 V [18]. Extensions beyond this are possible with organic electrolytes, but it is unlikely they will be found in the application space of wearable electrochemical sensing systems. These limitations on the usable potential of the electrochemical cell should be considered when selecting the voltage for the various power rails in the system. Common choices include 3 V, 3.3 V, and 5 V. The selected power rail must satisfy the requirements of measurement potential range, power efficiency, component supply requirements, and supply noise.

Enclosure

Wearable devices are exposed to a variety of environments and are subject to constant movement. To improve the usability and reliability of the system the electronics should be protected inside of an enclosure. Electrodes must frequently be replaced because of short lifetimes and to prevent cross contamination. As a result of this it is often desirable to have a quick connect mechanism on the enclosure that makes electrical contact with the electrodes without wired connections. Traditionally this was done by mounting an edge connector on the PCB and exposing it through a hole in the enclosure. These connectors are commercialized products and are readily available with a variety of predefined pitches and thicknesses. These connectors work well for thicker electrodes, but their use hindered by these same mechanical

constraints. New interface systems must be developed to make quick connections with the newer screen-printed and microneedle form factor sensors. For small batch production of enclosures 3D printing is the obvious choice. 3D printing drastically lowers the cost of using custom enclosures when compared to injection molded parts.

Continuous Glucose Monitor

Motivation

The goal of this project is to create a wearable, minimally invasive system for continuous monitoring of glucose in interstitial fluid (ISF). This system has also been designed to offer a second measurement channel which can be used to monitor other analytes or to double the sample size of the measurement. ISF is a desirable sensing medium due to the ease of access and correlated blood glucose concentration [19, 20]. ISF also lacks the coagulates that prohibit the continuous monitoring of blood glucose [21]. Monitoring glucose levels is critically important for the treatment of diabetes. Experts predict that over 500 million people will have diabetes in 2030, with the majority of these people living in low- and middle-income countries [22]. To combat this epidemic the best tool may be a wireless and non-invasive glucose continuous monitor. This device has the potential to allow doctors, parents and care givers to remotely monitor a patient's glucose level when they cannot be trusted to self-monitor. This capability would be particularly beneficial for parents with small children and for large hospitals that require the ability to economically monitor the glucose levels of multiple patients.

Sensor - Microneedle Array

ISF is accessed via an array of micron-sized needles which disrupt the outer layer of the skin. These needles are filled and coated to form a glucose selective electrochemical sensor. The working and reference needles employ a two-step fabrication scheme – each packed with a

conductive paste and interface wire. The counter needle is packed with carbon paste and uses a platinum wire, while the reference needle is filled with silver paste and uses a silver wire.

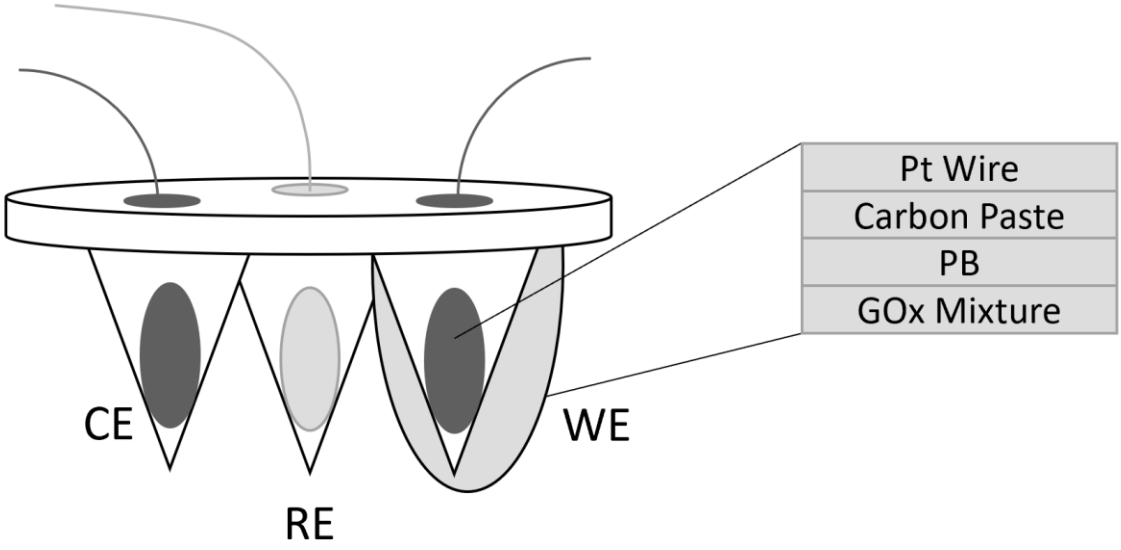

Figure 7: Microneedle array with working electrode detail

The working electrode requires a multistep fabrication process to create a glucose selective electrode. To create this electrode carbon paste is first used to fill the microneedle. The exposed carbon paste at the tip of the needle is coated with a layer of Prussian Blue (PB) via the electrodeposition. Next the enzyme, glucose oxidase (GOx) is stabilized and immobilized in a chitosan polymer. This polymer/enzyme mixture is then used to decorate the tip of the working electrode. This layered structure facilitates the detection of glucose through the pathway shown schematically in Figure 8.

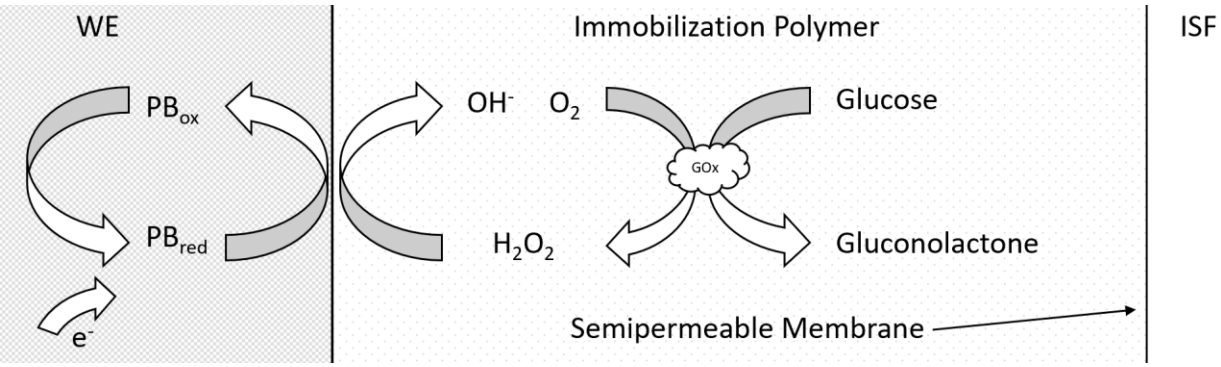

Figure 8: Schematic of enzymatic glucose detection.

The detection of glucose is a three-step reaction which follows these steps:

1. $Glucose + O_2 \xrightarrow{GOx} Gluconolactone + H_2O_2$
2. $H_2O_2 + PB_{red} \rightarrow H_2O + PB_{ox}$
3. $PB_{ox} + e^- \rightarrow PB_{red}$

GOx is used because of its inherent selectivity to glucose but direct charge transfer into the carbon paste working electrode is hindered by steric and kinetic factors [23]. To overcome this issue, a redox mediator is needed to transfer charge between the enzyme and electrode. The hydrogen peroxide (H_2O_2) produced by GOx is sensed, indirectly monitoring the glucose concentration. This is done through the amperometric detection of H_2O_2; however traditional unmodified electrodes are not selective to H_2O_2. An amperometric measurement under these conditions would show parasitic currents due to the readily oxidizable species in ISF which hinder the detection of H_2O_2. Prussian Blue (ferric hexacyanoferrate) is deposited under the conditions described by [24] to form a stable, highly active, and highly selective transducer for

H_2O_2. This reaction forms the final link in the diffusion limited reaction needed to detect glucose concentration with an amperometric measurement.

Electrical Specifications

This application requires long term continuous on body monitoring of glucose through small area electrodes. In addition, a second measurement channel is provided for monitoring other analytes in the future. To facilitate dual continuous measurements while remaining minimally invasive, a wireless bipotentiostat is desired. A bipotentiostat can be thought of as a two-channel version of a potentiostat. The bipotentiostat has a two-channel DAC, two potentiostat circuits, two transimpedance amplifiers, and a two-channel ADC. These duplicated subsystems allow for independent monitoring of two electrolytic cells – one measuring glucose concentration and the second reserved for future measurements. Due to the small area of the microneedle sensor a low, nanoamp, current range is expected. To facilitate a high measurement accuracy, a high-resolution DAC and ADC were selected instead of using MCU integrated peripherals. In general, the device was designed with measurement accuracy as the highest priority. The system is powered by a lithium ion battery and utilizes a low noise LDO to provide a stable 3.3 V supply. This supply is used for all system components. Using an LDO to create a 3.3 V power supply is desirable as it avoids larger, noise generating DC-DC switching regulators, but this choice limits the potential measurement range to about ±1.5 V. In this application this was acceptable as the potential required for the detection of glucose using the described enzymatic microneedle sensor is within this range.

System Design

The ADC selected for this application is the 4-channel, 24-bit, ADS122C04 made by Texas Instruments. The ADC is controlled via I2C and is capable of I2C transfer rates up to 1

Mbps (I2C Fast-Mode Plus). The ADS122C04 also integrates a programmable gain amplifier (PGA) and an internal 2.048 V reference. The PGA is leveraged to provide an extended measurement range and increase sensitivity when needed. The 24-bits of resolution maximize the measurement performance of the system but reduce the measurement bandwidth. Although this delta-sigma ADC has 24-bits of resolution, internal noise limits the effective number of bits to 20. Using the internal 2.048 V reference and the effective number of bits, each quantization step will be 1.95 µV and the maximum quantization error will be 976 nV. If a larger or symmetric sensing range is needed the ADC reference can be set to the 3.3 V power supply instead of the internal 2.048 V reference.

The DAC selected is the AD5667R, a two-channel, 16-bit DAC with an I2C interface made by Analog Devices. This DAC also has an integrated 1.25 V, 5 ppm/°C reference which is used throughout the system. Like the ADC, the quantization error of the DAC is an important design consideration. Using the 3V reference, the 16-bit DAC will have a quantization error of 45.7 µV. This low quantization error facilitates the use of measurement techniques that use a potential sweep. The low noise reference provided by the DAC is utilized to increase the level of system integration. This reference is buffered using a programmable analog block inside the MCU and routed to the potentiostat and TIA circuits where it is used as an offset. Since this is a single power supply system, the midpoint of the supply voltage is used to bias the op-amps. This facilitates the control and measurement of both positive and negative currents.

Each output channel of the DAC is fed into a dedicated reconstruction filter to remove the aliased images of the signal. The filter is constructed using a fourth order, unity gain, Sallen-Key topology [25]. The cut-off frequency of this low pass filter is set to 36 kHz. Both filters are

implemented using a four-channel op-amp – the MCP629, made by Microchip. This choice was made primarily to reduce the size of the board.

The maximum update rate of the DAC is limited by the highest common speed of all devices on the I2C bus. In this case, that speed is 400 kHz or 2.5 µS per bit. The largest amount of I2C traffic will occur when potential scanning measurements are running on each channel. This scenario is used to calculate the worst-case data throughput.

Table 1: Data Throughput for Single Channel Measurement

I2C Clock Speed	400 kHz	
Action	**Bits**	**Time**
DAC value update	36	90 µs
ADC start conversion	18	45 µs
ADC conversion time	N/A	520 µs
ADC read	55	138 µs
Total, 1 channel	109	793 µs

Table 1 shows that for each channel the maximum measurement frequency will be limited to 1.25 kHz. If both channels are running measurements that require a DAC update for every ADC reading the maximum measurement frequency will be 625 Hz. The data throughput is the limiting factor in the linear sweep rate specification of the system. The linear sweep rate of the system is 12.5 V s^{-1} using 10 mV steps and 1.25 V s^{-1} using 1 mV steps. This sweep rate is acceptable for this application but could be further improved by moving the DAC and ADC onto dedicated I2C busses. If the components are moved onto dedicated busses the ADC can be run at 1 MHz and the DAC at 400 kHz. If the DAC is operated at its maximum resolution the quantization error will be 22.6 µV. This is ample accuracy for this application and will support future applications.

The op-amp used in the transimpedance amplifier is the MAX44280, a low noise, low-offset, rail-to-rail op-amp made by Maxim Integrated. This part has a typical input bias current of 10 fA at 25 °C and a typical input voltage offset of 10 µV. These characteristics, when combined with a 50 MHz bandwidth, 1.2 fA $Hz^{-0.5}$ input current noise density, and small 1.5 mm x 1 mm package make this an ideal part for this application. The downside of using this part is that it is not unity gain stable. Ideally the same op-amp could be used in both the transimpedance amplifier and control circuit but because the control circuit uses unity gain amplifiers, this part cannot be used without external compensation. The internally compensated LMV881, from Texas Instruments, was used for the reference buffer and control amplifier since it is unity gain stable.

The system is controlled by a PSoC 4200 BLE microcontroller made by Cypress Semiconductor. This part combines a Cortex-M0 CPU, BLE radio, and reconfigurable digital and analog blocks. This part was primarily selected because of these features. The reconfigurable analog blocks are leveraged to create a buffer for the reference voltage without adding additional op-amps. The integrated BLE radio provides a space efficient wireless communication link and is easily configured using the free integrated development environment, PSoC Creator, provided by Cypress. This family of parts comes is available in a variety of pinouts with a wide feature set. The specific part used in this design is the CY8C4247LQI-BL483, a 56-pin QFN with 128 kB of flash memory.

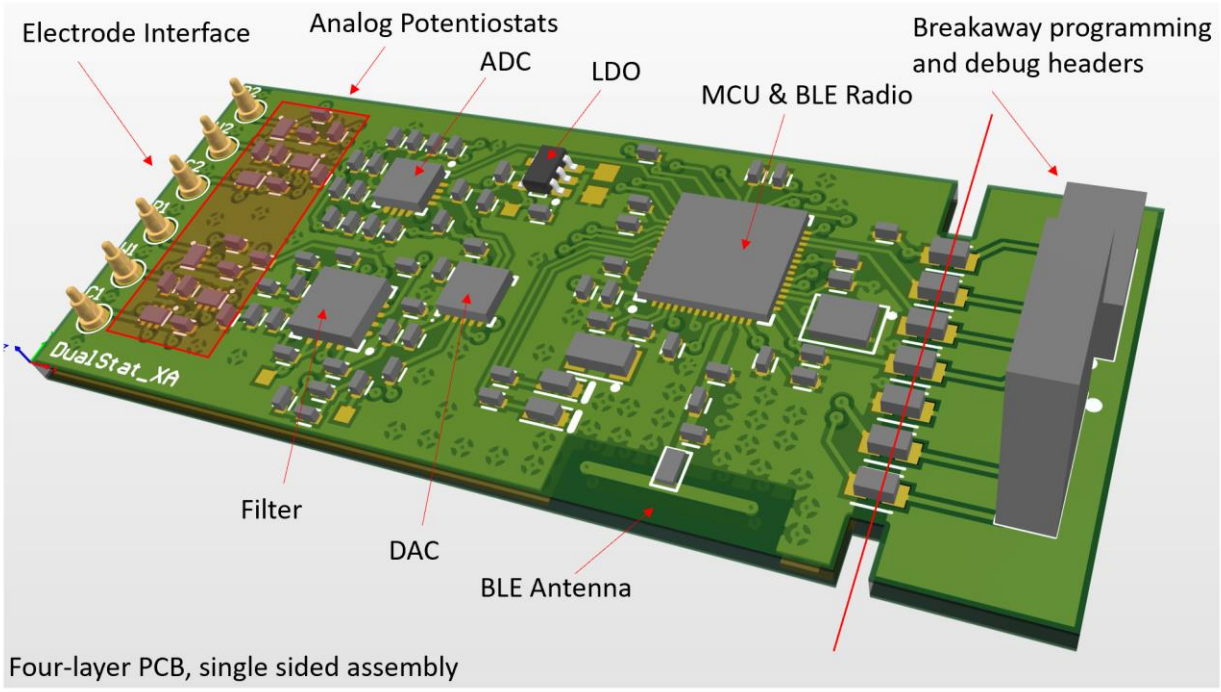

Figure 9: Annotated electronics

Figure 9 shows a rendering of the electronics created in Altium, a PCB design tool. Notable subsystems include the electrode interface, analog potentiostats, ADC, regulator, MCU, BLE radio and antenna, DAC, and reconstruction filter. The PCB is a four-layer board with components on a single side. The PCB was designed with dedicated ground and power layers to help reduce noise and improve BLE performance. The PCB was also designed with a breakaway extension which houses programming and debug headers to reduce system size after development is completed.

The quick connect interface is implemented using spring loaded pogo-pins. The pins are aligned with conductors on the electrodes and held in place by a 3D printed enclosure to make the electrical connection between the potentiostat and the sensor. The 3D printed enclosure is shown in Figure 10.

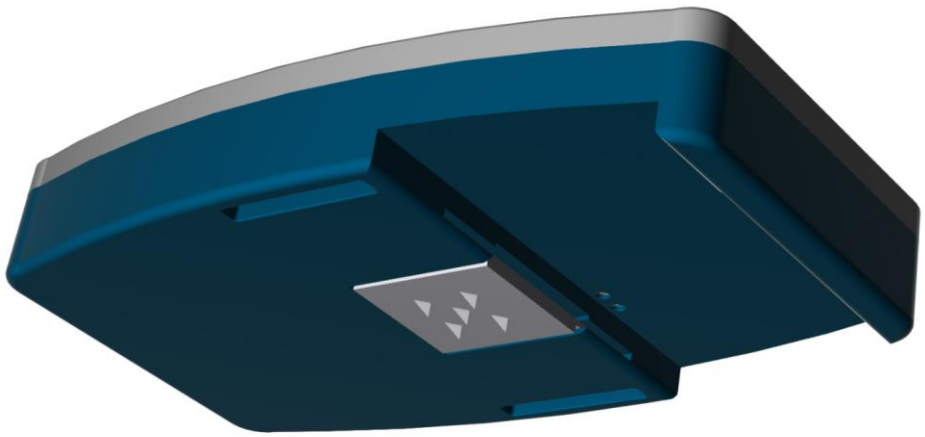

Figure 10: Model of 3D Printed Enclosure

System Evaluation Methods

The performance of the electronics in the system are evaluated using a two-step process common in professional quality management systems. The initial phase is verification where each subsystem is analyzed to ensure that it is working as designed. The second stage is validation during which the entire system is analyzed to ensure it meets the functional specifications.

Verification

After receiving the assembled potentiostat electronics, they were visually inspected with a microscope. During this inspection the system was checked for missing components, incorrectly installed components, and solder bridges. Following the inspection, the device was powered with a DC power supply at 4V and the LDO output voltage was verified.

To assist in the hardware verification, the potentiostat circuit and the transimpedance amplifier were simulated using a SPICE simulator (LTSpice, Analog Devices). The simulated

circuit uses a spice model of the MAX44280 provided by Maxim Integrated to model the circuit with a higher degree of accuracy than what ideal op-amp models can provide. Transient simulations were run to check voltages throughout the potentiostat and transimpedance amplifier circuits. The simulated voltages were checked against the voltages found on the board to identify faulty components.

A single test is used to verify that all major system components, being the MCU, DAC, and ADC, are functioning as expected. The counter electrode is connected directly to the reference electrode and a resistor is placed between the counter/reference electrode and the working electrode to simulate a simple electrochemical cell. A li-ion battery or equivalent power source is connected to supply power. To complete the experimental setup the MCU is programmed and a TTL-to-USB cable is connected between the potentiostat and a test computer. A terminal emulator (Tera Term or equivalent) is used to send commands and receive data from the potentiostat. This test uses Ohm's Law as a check to make sure that the potential generated by the DAC and current measured by the ADC is linear across the entire measurement range. The resistance between the working and counter/reference electrodes is calculated by fitting a linear trend line to the potential vs current data. This experiment also provides a way to calibrate the system for offsets and to analyze the linearity of the system across the current range. The results of two of these tests are shown in Figure 11.

Table 2: Initial verification - resistor test error

Trial	Actual Resistance	Calculated Resistance	Percent Error
30k	29880	30.739	2.87%
360k	358600	347230	3.17%

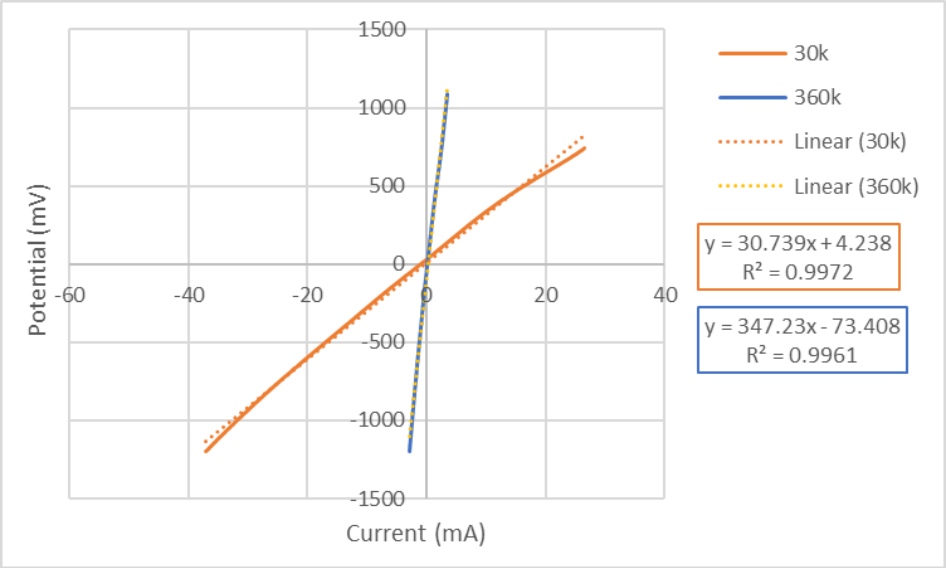

Figure 11: Initial verification – resistor test results

The BLE radio was verified by connecting to the device from a generic BLE scanner (Light Blue, Punch Through Design) and reading characteristics that were configured in the firmware. Notifications were also sent from the potentiostat to the phone. An iOS application is planned as the final configuration and data visualization interface for this wearable device.

Validation

To validate the electronic aspect of the system, a simplified experiment is conducted using a screen-printed electrode modified with Prussian Blue ink. The screen-printed electrode is used as the initial sensor because it is readily available and produces larger currents due to its large surface area (with respect to a microneedle). The Prussian Blue modification to the working electrode acts as an "artificial peroxidase" making a hydrogen peroxide selective electrode [24]. This experiment is a short-circuited version of the full glucose detection pathway and provides a simplified starting point. This experimental setup is preferred since it eliminates glucose oxidase and any enzymatic issues. This sensor is used to run an amperometric calibration experiment which measures the concentration of hydrogen peroxide through direct reduction on

the Prussian Blue modified electrode. In this experiment, concentrations of hydrogen peroxide ranging from 0-1.1mM H_2O_2 are measured in a chronoamperometric measurement with a potential of -250 mV. A linear relationship between the measured current and concentration of hydrogen peroxide is expected. The results from this test are shown in Figure 12. Figure 12 shows two baseline trials with 0.1 M PBS followed by four trials of increasing concentrations of hydrogen peroxide. As more hydrogen peroxide is added, the steady state current increases in magnitude.

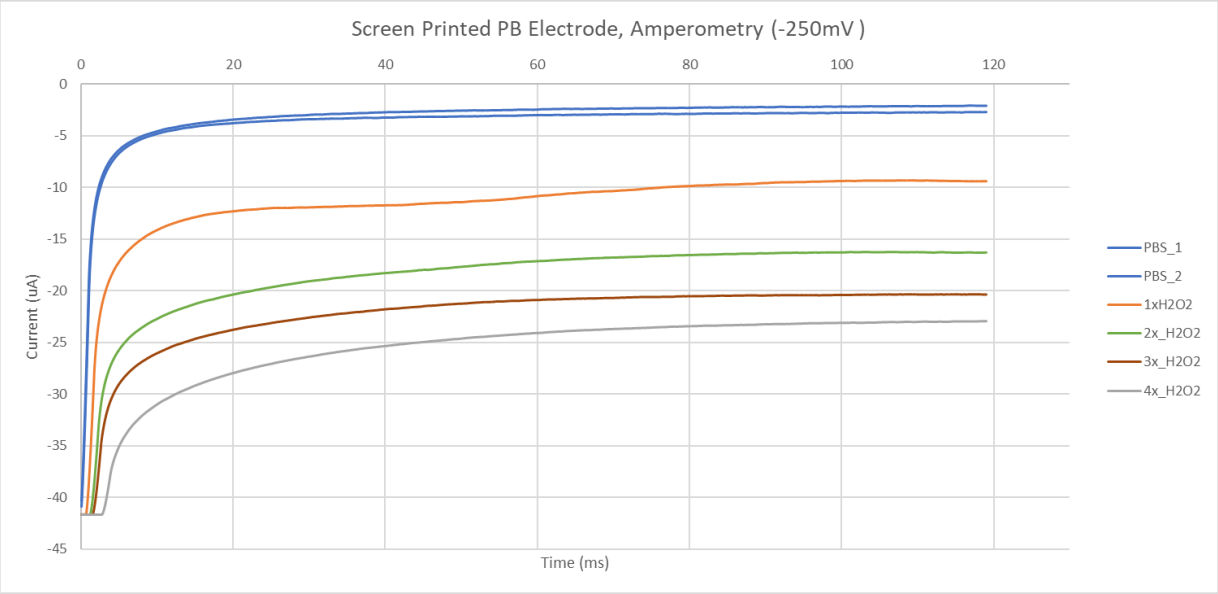

Figure 12: Amperometric Calibration of Screen-Printed Electrode

The linearity of this experiment is shown in Figure 13. The data is fit to a linear trendline with a R^2 value of 0.9786. This trend shows that increasing concentrations of hydrogen peroxide increase the magnitude of the amperometric current as expected. In Figure 13 and all other linearity plots, the steady state current is calculated by averaging the final 20 seconds of data.

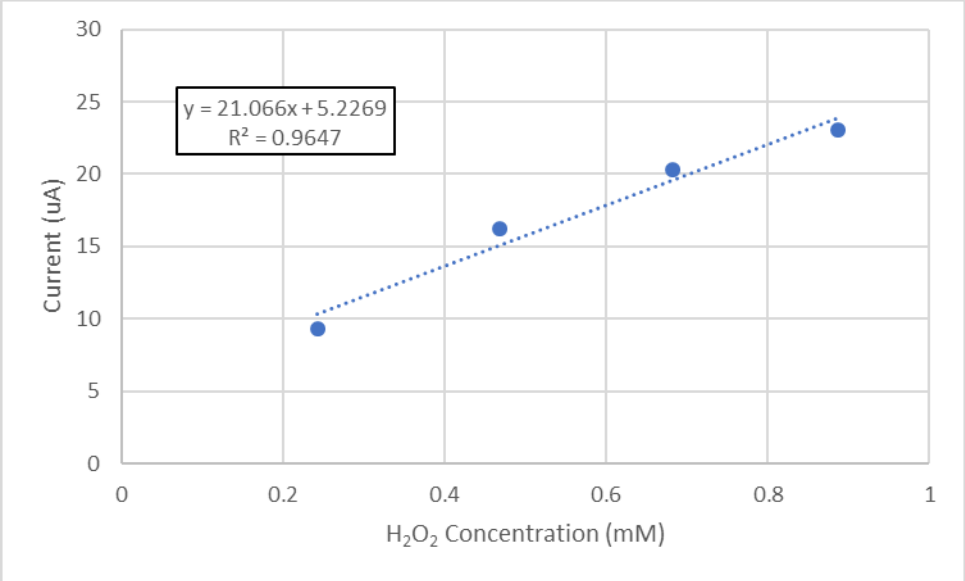

Figure 13: Calibration Linearity for Screen-Printed Electrode

After the successful test of the large screen-printed electrode, the gain of the transimpedance amplifier was increased from 30 kΩ to 600 kΩ for use with microneedles. The working and counter electrodes of the microneedles were prepared by following the initial steps in the procedure outlined in Figure 8. The final step of fabrication – the addition of GOx polymer was omitted to reduce measurement complexity. Additionally, an external silver/silver chloride wire was used as a reference. This choice was made to add a level of redundancy to the microneedle fabrication. The microneedle array used was made with one counter electrode and two working electrodes. This creates a redundant working electrode that is be used in case of failure. The same calibration experiment was run with PB modified microneedles to test the systems performance under these more demanding conditions.

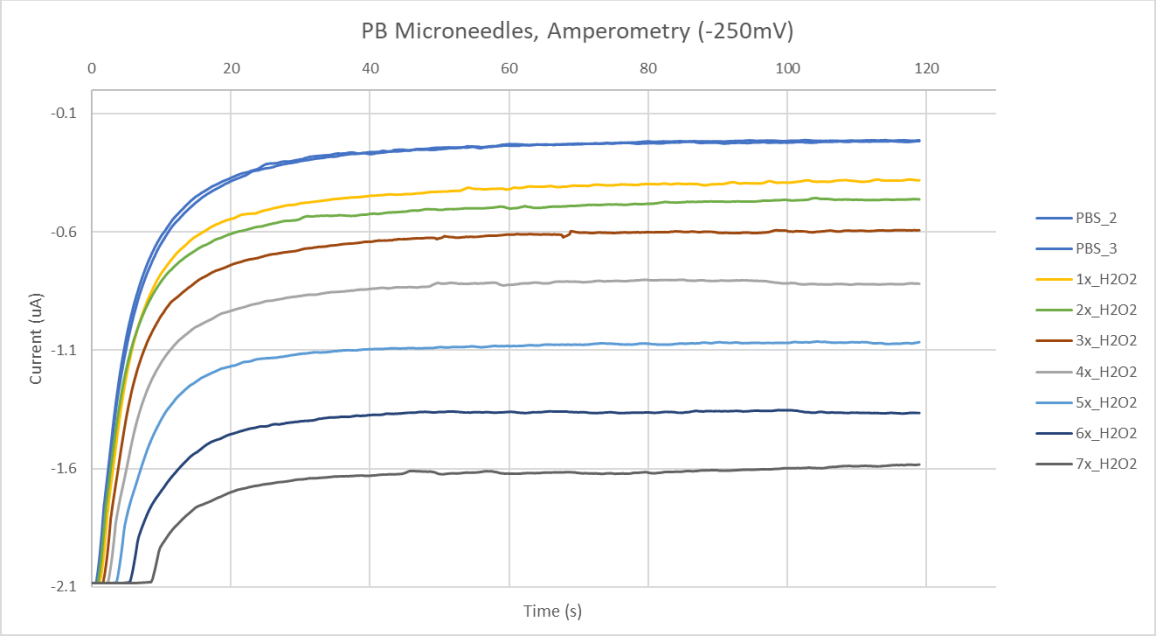

Figure 14: Amperometric Calibration of Prussian Blue Microneedle Array

The results of this testing closely mirror the results of the screen-printed electrode test. The system is linear and has a similar R^2 value of 0.9627. This test was run with increasing concentrations of H_2O_2 up to a maximum concentration of 4 mM H_2O_2.

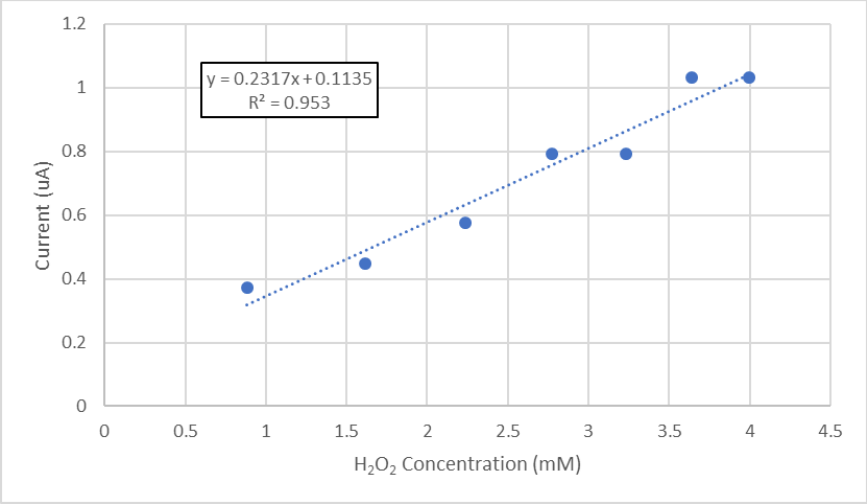

Figure 15: Calibration Linearity of Prussian Blue Microneedle Array

The amperometric calibration of Prussian Blue microneedles was repeated on a DStat which is an open source potentiostat capable of precision similar to that of a commercial bench

top potentiostat [26]. The DStat amperometric curves shown in Figure 16 are much smoother which is due to the improved noise rejection of the DStat. The DStat test was used to determine if the non-linearity observed in the previous calibration test was due to the electronics or the sensor. The similarities between the linearity plots in Figure 15 and Figure 17 suggests that the non-linearity observed may be coming from the sensor and not the electronics. Additional testing and statistical analysis are needed before this can be conclusively claimed.

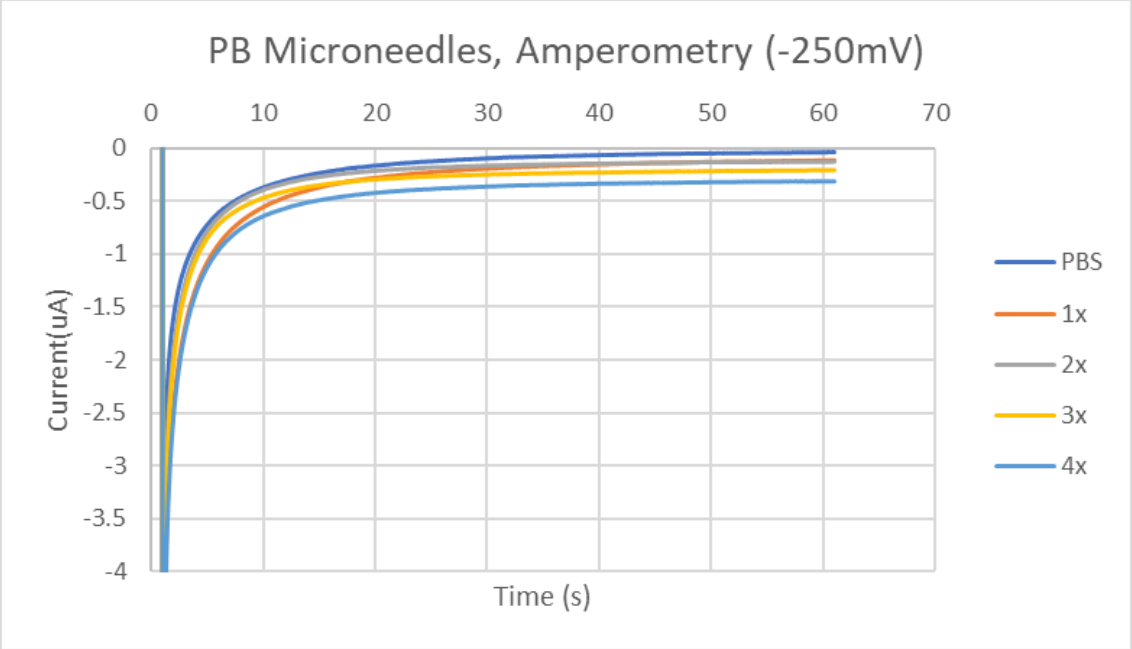

Figure 16: DStat Amperometric Calibration of Prussian Blue Microneedle Array

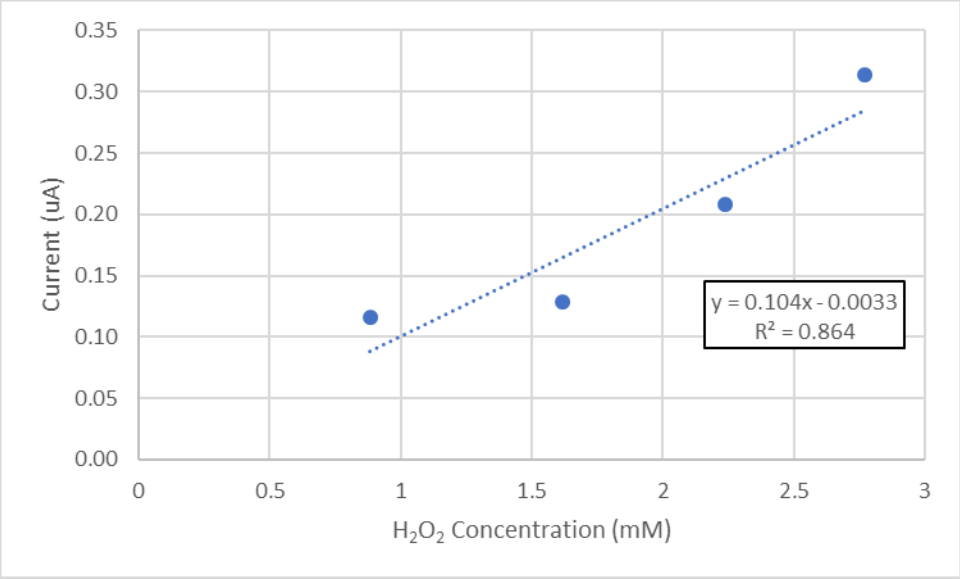

Figure 17: DStat Calibration Linearity of Prussian Blue Microneedle Array

Although not needed to test the electronics, a final test was conducted using a prototype microneedle array which had undergone the complete modification to create a glucose selective sensor. The results from this test are shown in Figure 18 and 19. The large abrupt changes in the current seen in Figure 18 may be due to vibration or popping bubbles which disrupt the diffusion limited mode of the reaction. The microneedles are tested by applying a drop of solution directly to the tip and as a result are quite sensitive to movement which introduces another mode of mass transport to the reaction. Even with the poor R^2 value and noisy data, the amperometric response is valuable since it validates the complete detection reaction.

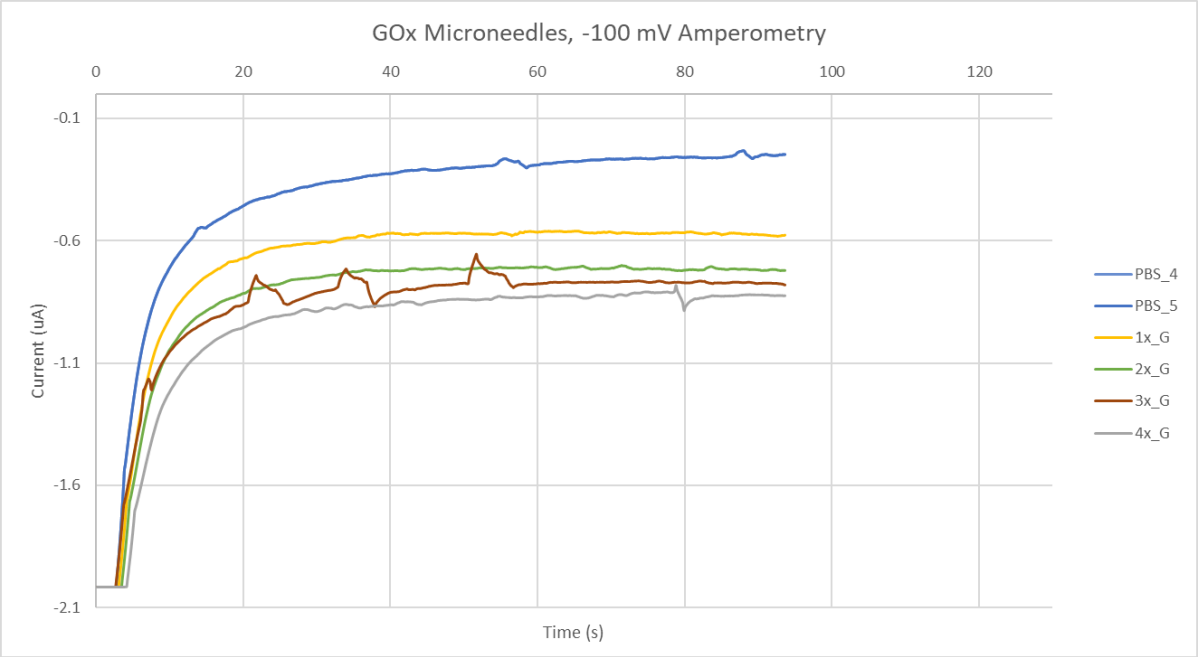

Figure 18: Amperometric Calibration of GOx Microneedle Array

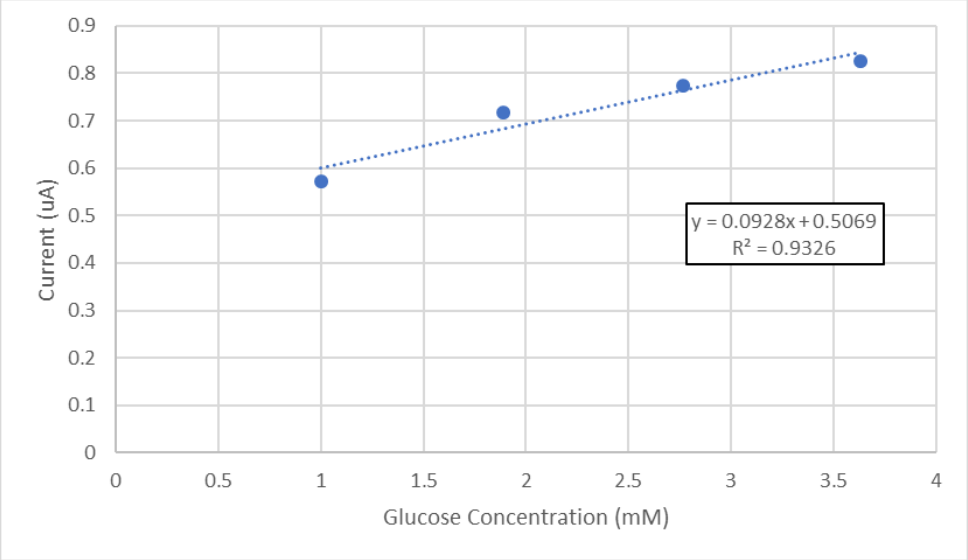

Figure 19: Calibration Linearity of GOx Microneedle Array

Future Work

The electronics evaluated in this work are the first revision of this design. Testing has uncovered an area that will need to be improved in the next revision of the system. As designed, the wearable bipotentiostat suffers from instability. Stability is an intrinsic problem in

potentiostats due to the capacitive nature of electrochemical sensors. Furthermore, any resistance at the reference electrode will increase the phase shift caused by the capacitance. This capacitance introduces instability by causing a phase shift in the feedback loop of the control amplifier. If this phase shift is large enough it can cause positive feedback instead of the intended negative feedback. This has led many of the commercial potentiostat companies to publish white papers and write guidelines on improving the stability of the system [27-30]. There are a variety of solutions available that will need to be investigated before the next revision is built.

Conclusion

Even though improvements are still needed to improve the stability of the wearable potentiostat designed in this paper, it is still a useful tool in its current state. Results shows that it is capable of measuring analyte concentration using a small area microneedle array at sub mM concentration levels. The development of this potentiostat will continue until all design goals have been achieved.

Bibliography

[1] J. E. Mück, B. Ünal, H. Butt, and A. K. Yetisen, "Market and Patent Analyses of Wearables in Medicine," *Trends in Biotechnology*, vol. 37, no. 6, pp. 563-566, 2019/06/01/ 2019.

[2] M. P. Turakhia, M. Desai, H. Hedlin, A. Rajmane, N. Talati, T. Ferris, S. Desai, D. Nag, M. Patel, P. Kowey, J. S. Rumsfeld, A. M. Russo, M. T. Hills, C. B. Granger, K. W. Mahaffey, and M. V. Perez, "Rationale and design of a large-scale, app-based study to identify cardiac arrhythmias using a smartwatch: The Apple Heart Study," *American Heart Journal*, vol. 207, pp. 66-75, 2019/01/01/ 2019.

[3] R. K. Mishra, A. M. Vinu Mohan, F. Soto, R. Chrostowski, and J. Wang, "A microneedle biosensor for minimally-invasive transdermal detection of nerve agents," *Analyst*, vol. 142, no. 6, pp. 918-924, 2017.

[4] J. Kim, A. S. Campbell, and J. Wang, "Wearable non-invasive epidermal glucose sensors: A review," *Talanta*, vol. 177, pp. 163-170, 2018.

[5] G. A. Evtugyn, H. C. Budnikov, and E. B. Nikolskaya, "Sensitivity and selectivity of electrochemical enzyme sensors for inhibitor determination," vol. 46, no. 4, pp. 465-484, 1998.

[6] F. C. Walsh, L. F. Arenas, and C. Ponce de León, "Developments in electrode design: structure, decoration and applications of electrodes for electrochemical technology," *Journal of Chemical Technology & Biotechnology*, vol. 93, no. 11, pp. 3073-3090, 2019/05/13 2018.

[7] A. J. Bard and L. R. Faulkner, *Electrochemical Methods: Fundamentals and Applications*, Second Edition ed. John Wiley & Sons, Inc., 2001.

[8] P. M. Biesheuvel and J. E. Dykstra, "The difference between Faradaic and Nonfaradaic processes in Electrochemistry," p. arXiv:1809.02930, 2018.

[9] F. C. Strong, "Faraday's laws in one equation," *Journal of Chemical Education*, vol. 38, no. 2, p. 98, 1961/02/01 1961.

[10] J. Wang, "Glucose Biosensors: 40 Years of Advances and Challenges," *Electroanal*, vol. 13, no. 12, pp. 983-988, 2001.

[11] K. Rathee, V. Dhull, R. Dhull, and S. Singh, "Biosensors based on electrochemical lactate detection: A comprehensive review," *Biochemistry and Biophysics Reports*, vol. 5, pp. 35-54, 2016/03/01/ 2016.

[12] B. Bohunicky and S. A. Mousa, "Biosensors: the new wave in cancer diagnosis," (in eng), *Nanotechnol Sci Appl,* vol. 4, pp. 1-10, 2010.

[13] N. N. Nik Mansor, T. T. Leong, E. Safitri, D. Futra, N. S. Ahmad, D. N. Nasuruddin, A. Itnin, I. Z. Zaini, K. T. Arifin, L. Y. Heng, and N. I. Hassan, "An Amperometric Biosensor for the Determination of Bacterial Sepsis Biomarker, Secretory Phospholipase Group 2-IIA Using a Tri-Enzyme System," (in eng), *Sensors (Basel),* vol. 18, no. 3, p. 686, 2018.

[14] Gamry and I. Instruments, "Two-, Three-, and Four-Electrode Experiments," Rev. 3.0 ed. https://www.gamry.com/assets/Uploads/2-3-4-Electrodes-rev-3a.pdf, 2015.

[15] L. Busoni, M. Carla, and L. Lanzi, "A comparison between potentiostatic circuits with grounded work or auxiliary electrode," (in English), *Review of Scientific Instruments,* vol. 73, no. 4, pp. 1921-1923, Apr 2002.

[16] R. Doelling, "Potentiostats," in "Bank Elektronik Application Note," Bank Elektroni–Intelligent Controls GmbH, Clausthal-Zellerfeld, Germany, 2000, [Online]. Available: http://www.bank-ic.de/encms/downloads/potstae2.pdf.

[17] B. D. McCloskey, "Expanding the Ragone Plot: Pushing the Limits of Energy Storage," *J Phys Chem Lett,* vol. 6, no. 18, pp. 3592-3, Sep 17 2015.

[18] L. Smith and B. Dunn, "Batteries. Opening the window for aqueous electrolytes," *Science,* vol. 350, no. 6263, p. 918, Nov 20 2015.

[19] S. N. Thennadil, J. L. Rennert, B. J. Wenzel, K. H. Hazen, T. L. Ruchti, and M. B. Block, "Comparison of Glucose Concentration in Interstitial Fluid, and Capillary and Venous Blood During Rapid Changes in Blood Glucose Levels," *Diabetes Technology & Therapeutics,* vol. 3, no. 3, pp. 357-365, 2001.

[20] E. Cengiz and W. V. Tamborlane, "A tale of two compartments: Interstitial versus blood glucose monitoring," *Diabetes Technology and Therapeutics,* Article vol. 11, no. SUPPL.1, pp. S11-S16, 2009.

[21] P. P. Samant and M. R. Prausnitz, "Mechanisms of sampling interstitial fluid from skin using a microneedle patch," *Proc Natl Acad Sci USA,* vol. 115, no. 18, p. 4583, 2018.

[22] D. R. Whiting, L. Guariguata, C. Weil, and J. Shaw, "IDF Diabetes Atlas: Global estimates of the prevalence of diabetes for 2011 and 2030," *Diabetes Research and Clinical Practice,* vol. 94, no. 3, pp. 311-321, 2011/12/01/ 2011.

[23] L. Gorton, "Carbon paste electrodes modified with enzymes, tissues, and cells," *Electroanal*, vol. 7, no. 1, pp. 23-45, 1995.

[24] A. A. Karyakin, E. E. Karyakina, and L. Gorton, "Amperometric Biosensor for Glutamate Using Prussian Blue-Based "Artificial Peroxidase" as a Transducer for Hydrogen Peroxide," *Analytical Chemistry*, vol. 72, no. 7, pp. 1720-1723, 2000/04/01 2000.

[25] "Analysis of Sallen-Key Architecture," Texas Instruments, 2002, [Online]. Available: http://www.ti.com/lit/an/sloa024b/sloa024b.pdf.

[26] M. D. M. Dryden and A. R. Wheeler, "DStat: A Versatile, Open-Source Potentiostat for Electroanalysis and Integration," *PLOS ONE*, vol. 10, no. 10, p. e0140349, 2015.

[27] I. Gamry Instruments. (2019). *Tips and Techniques for Improving Potentiostat Stability* [Online]. Available: https://www.gamry.com/application-notes/instrumentation/potentiostat-stability-tips-techniques/.

[28] P. M. Nawghare, "Optimum Compensation and Stability of Potentiostat," *International Journal of Electronics Engineering*, vol. 1, 1, pp. 1-6, 2009.

[29] (2018). *Potentiostat stability mystery explained* [Online]. Available: https://www.bio-logic.net/wp-content/uploads/Application-note-4.pdf.

[30] A. Bewick and M. Fleischmann, "The design and performance of potentiostats," *Electrochimica Acta*, vol. 8, no. 3, pp. 89-106, 1963/03/01/ 1963.